2023 IEEE International Conference on Robotics and Automation (ICRA 2023)
May 29 - June 2, 2023. London, UK

# Compliant Finger Joint with Controlled Variable Stiffness based on Twisted Strings Actuation

Mihai Dragusanu[1*], Danilo Troisi[1,2*], Domenico Prattichizzo[1,3] and Monica Malvezzi[1]

***Abstract*— Underactuated tendon-driven fingers are a simple, yet effective solution, for realizing robotic grippers and hands. The lack of controllable degrees of actuation and precise sensing is compensated by the deformable structure of the finger, which is able to adapt to the objects to be grasped and manipulated, and also to implement grasping strategies based on environmental constraint exploitation. One of the main drawbacks of these robotic fingers is that, due to the limited number of actuators, they can only realize a limited number of movements. Finger closure motion realized by activating the tendon depends on finger mechanical properties, and in particular on elastic joint stiffness. In this paper, we introduce a passive elastic joint to be implemented in monolithic fingers in which the stiffness can be actively regulated by applying a pre-compression to the structure, controlled by a twisted-string actuator (TSA). The paper describes the working principle of the joint, investigates the relationship between pre-compression and flexural stiffness, and finally shows its application to a robotic finger composed of three phalanges.**

## I. Introduction

Robotic grippers and hands are the main end-effectors that robots use for interacting in the environment, for grasping and manipulating objects. Grasping and manipulation have challenged robotics researchers and engineers from the beginning, and, notwithstanding a large amount of literature and devices available, the problem is still open. Advancements in new materials and technology, as well as in the efficient design of highly deformable structures have supported an increasing interest in developing soft robotic grippers [1] and hands [2], [3]. Soft manipulation is a particularly effective solution in unstructured and uncertain operative environments, since it overcomes the sensing limitations in defining object location and shape. Soft hands and grippers are simply closed over the object and the intrinsic compliance allows the hand to adapt to different object shapes [4]. Inspired by human manipulation, soft gripper and hands can furthermore exploit environmental constraints for compensating the lack of controllable degrees of freedom [5], [6]. Hand compliance properties, and in particular joint stiffness, play an important role in defining the properties of a robotic grasp [7], [8].

The methodology at the base of the work presented in this paper was introduced in [9], in which underactuated tendon-driven robotic fingers composed of rigid and compliant modular elements were considered, and where the stiffness of compliant joints was evaluated to obtain a given closure motion for the finger. Elastic joints were manufactured with a soft material and the stiffness could be regulated in the manufacturing phase by controlling the infill density percentage. The methodology was extended in [10] to interpenetrating phase composites materials, while in [11] it was applied to monolithic fingers with wave-shaped elastic joints where the elastic properties could be regulated by changing joints' geometrical shape and dimension. In [11], furthermore, the methodology was extended to other tasks apart from finger closure motion. The mentioned works proposed a methodology for designing passive joint stiffness according to specific task requirements, but, once the robotic finger is manufactured and assembled, these parameters could not be regulated anymore.

In this work, we seek to overcome this limitation by proposing a way for controlling and adapting finger joint stiffness beyond its fabrication and assembly, during gripper operative life. We started from the monolithic soft-rigid finger structure based on wave-joints [11], introducing a new

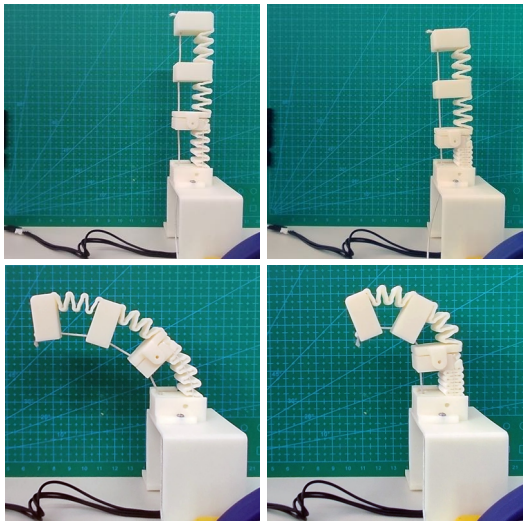

Fig. 1: Underactuated tendon-driven robotic finger structure based on wave-joints presented in [11], in which the proximal joint stiffness can be regulated by means of a TSA system. Top images: unactuated finger with different stiffness values in the proximal joint (softer on the left, harder on the right). Lower images: corresponding finger closure motions. Acting on the TSA actuator it's possible to regulate finger closure motion.

[1]are with the Department of Information Engineering and Mathematics, University of Siena, Siena, Italy {dragusanu, troisi, prattichizzo, malvezzi}@diism.unisi.it.

[2]are with the Department of Information Engineering, University of Pisa, Pisa, Italy {danilo.troisi@phd.unipi.it}

[3]are with the Department of Advanced Robotics, Istituto Italiano di Tecnologia, Genova, Italy. {domenico.prattichizzo}@iit.it

*Equally contributed to this work.

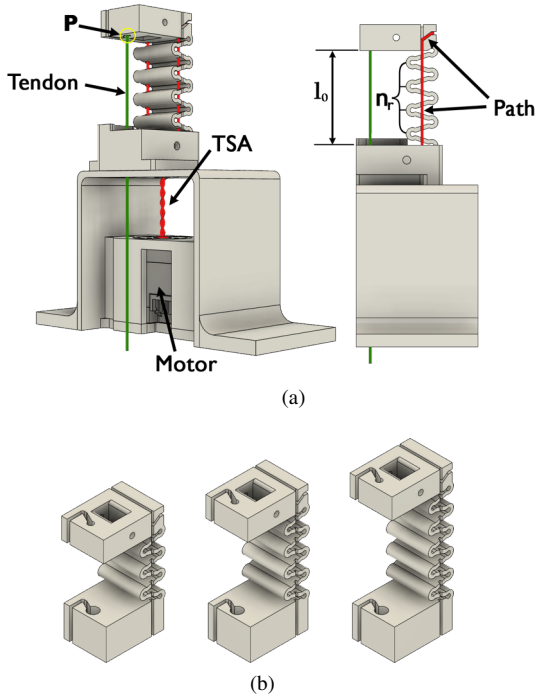


(a)

(b)

Fig. 2: CAD model of a wave-joint with variable stiffness. (a) The joint is actuated by the green tendon, which is connected to a motor, while joint flexural stiffness is regulated by the TSA (red tendon), which by pulling the extremities of the joint, compresses the wave, increasing its stiffness. The joint stiffness is regulated by controlling the TSA stroke. (b) The three modules considered in this study, with $n_r$ equal to 3, 4 and 5.

system, based on TSA (twisted string actuation), for regulating joint stiffness, obtained by applying a pre-compression of the joint. The pre-compression, applied by a twisted string actuator, introduces a stress/deformation state in the joint that modifies its flexural stiffness and therefore, according to [9], modify finger closure motion and grasping capabilities. The main contribution of the paper is therefore the combination of a compliant tendon-driven finger with a TSA, that controls elastic joint stiffness.

In the paper, the system for pre-compressing flexible joints by means of the TSA is presented. The relationship between pre-compression and flexural stiffness in single wave-joints is investigated firstly by means of FEM-based numerical simulations, and then by means of an experimental setup. To demonstrate the applicability of the proposed solution in robotic grippers and hands, a set of closure movement experiments has been realized with a tendon-actuated finger composed of three phalanges (Fig. 1).

## II. Methodology

In this section, we introduce the variable-stiffness wave-shaped elastic joint, analyze it by means of numerical simulations and present the experimental setup realized for joint characterization.

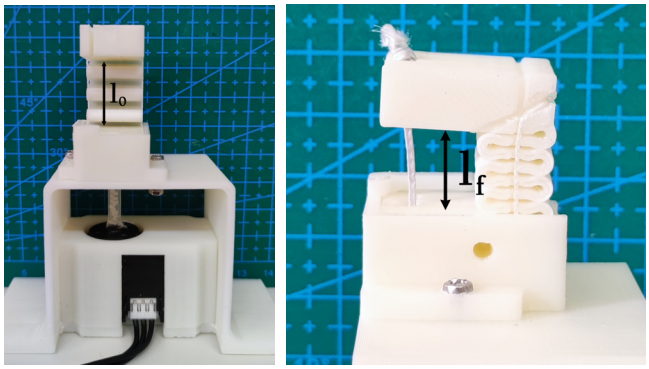


(a) (b)

Fig. 3: Prototype of the wave-joint with variable stiffness for the identification of stiffness properties (a) frontal view, where the TSA for joint stiffness regulation is evident, the joint is in its initial configuration, with length $l_0$. (b) lateral view of the prototype with the wave-joint completely compressed, so that its length has been reduced to $l_f$.

### A. The wave-joints

The monolithic soft-rigid finger structure is composed of compliant wave-shaped elements, i.e. the wave-joints [11]. Each compliant finger element has a simple sinusoidal wave-shape created and parametrically defined by using CAD software as a function of a few parameters. The selected joint structure allows using the same material for both the flexible and rigid parts of the finger so that the whole finger can be realized as a single component, simplifying the assembly phase. By varying in the pre-processing phase of finger fabrication a limited set of parameters (joint length, wave height, number of ridges, wave thickness, and twist angle), it is possible to obtain the equivalent stiffness values needed to accomplish a specific task.

In this work, we introduce a further element for regulating joint stiffness, namely joint pre-compression produced by TSA. This element allows to actively change the joint stiffness after its fabrication, in a controllable way. To show the effect of the pre-compression induced by TSA, in this work we initially focused on a single joint, where we kept all the parameters unchanged (i.e. equal to the initial value described in [11]) except the number of ridges $n_r$ and, consequently the joint length.

With respect to the work presented in [11], we have slightly modified the structure of the wave-joint to route the tendons of the TSA used to vary the stiffness. Fig. 2 shows the CAD of the new wave-joint module and the inserted TSA. The new joint has a path inside, specially made to route the tendons. The tendon was folded in two parts and on one side it was twisted, passed inside a flexible tube, and fixed to the motor shaft, while on the other side it was routed through the compliant element following the path as shown in Fig. 2.

A TSA has been used to apply the pre-compression to

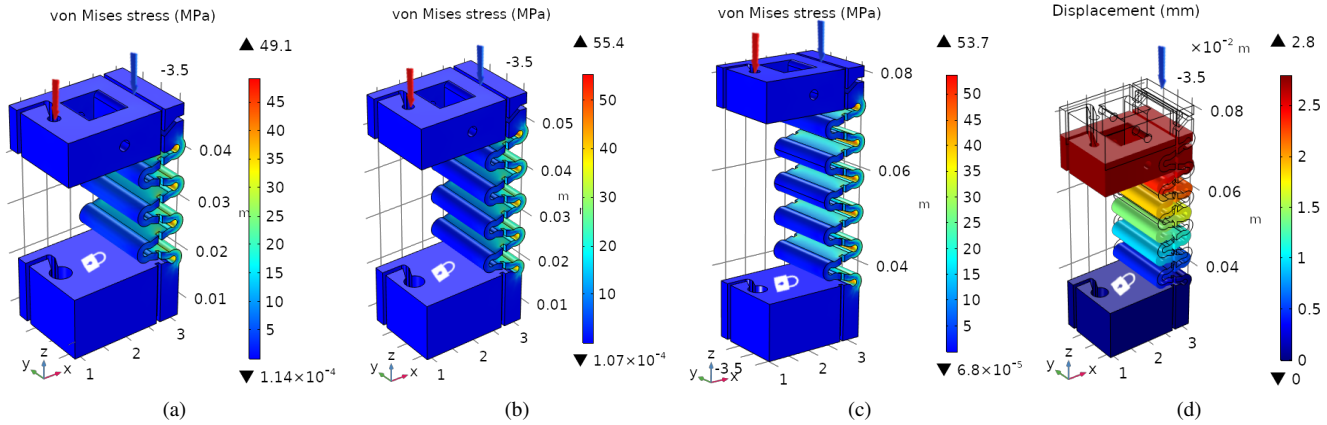


Fig. 4: A subset of FEM analysis results. Deformation obtained by applying a force simulating the TSA to the three considered joints: (a), (b), (c). Results obtained by applying a joint pre-compression and an actuation force to the tendon: (d).

the joint. The principle behind the TSA is very simple: it converts the rotary motion into linear through the twisting of two or more parallel strings that are connected on one side to a rotary motor on the other to a linear moving element, i.e. the load to be actuated. The electrical motor's rotation of the strings shortens them, creating a linear motion on the load side. In [12], [13] the TSA system's kinematics and dynamics model is presented. Thanks to the TSA characteristics, a small-size motor with high speed and low torque can be used to create a very high force and, moreover, a cheap, lightweight, and compact linear transmission system [14], [15]. In this study, a polyethylene (Dyneema fiber, Japan) cable was used due to its good strength with limited weight. The motor was positioned perpendicular to the joint tip so that the forces exerted by the twisted strings are distributed vertically on the structure.

Concerning the wave-joints, as previously mentioned, the only parameter that has been changed in this paper, to investigate the role of TSA, is the number of ridges and consequently also the overall length of the compliant module. Specifically, three case studies were considered, i.e. with $n_r = [3, 4, 5]$, and consequently an initial length $l_0 = [30\,\mathrm{mm}, 36\,\mathrm{mm}, 42\,\mathrm{mm}]$, respectively. This set of values has been chosen to be sufficiently representative and manageable in the identification procedure described in the following section in terms of data amount. Each compliant wave-joint consists of a single module 3D-printed in Acrylonitrile Butadiene Styrene (ABS). Each sample is composed of a rigid part, the cubes and a compliant part i.e. the waves. Moreover, in addition to the path designed to take advantage of the TSA, a further path on the cube edge (**P** in Fig. 2), allows to insert the tendon for actuating the joint flexion. In Fig. 3 the wave-joint sample with $n_r = 3$ and $l_0 = 30\,\mathrm{mm}$ is shown.

### *B. Preliminary investigation with numerical simulation*

A numerical structural analysis was set to determine if the twisted string actuator's action is able to provide a pre-compression suitable to control joint stiffness. The analysis, based on Finite Element Method (FEM), was conducted with COMSOL Multiphysics® software. The CAD model described above has been used for structural analysis.

A series of structural static tests has been performed to verify that the routing designed for the TSA is suitable to apply a pure compression deformation and to preliminary set the relationship between joint pre-compression joint deformation and stiffness properties.

Fig. 4d shows a representative set of results for one of the three case studies. The force, indicated by the blue arrow in Fig. 4d, acts in the vertical direction on the wave-shape structure simulating the TSA while the constrained part is the cube defined with a white padlock. From these results it can be verified that the applied force simulating the TSA causes a compression of the joint, without bending and buckling effects, and these preliminary results confirm that the tendon routing designed for the joint is correct.

Another set of preliminary tests on the three samples was performed to evaluate the maximum pre-compression and the maximum force required to flex the joint in the most critical scenario, with the highest joint stiffness.

From these preliminary tests it was found that the maximum force that can be applied to the TSA is $5\,\mathrm{N}$ for all the three samples, and the obtained maximum deformation (compression) values are $6\,\mathrm{mm}$, $8\,\mathrm{mm}$ and $12\,\mathrm{mm}$ for $n_r = [3, 4, 5]$, respectively. Fig. 3 shows the experimental results of the preliminary test for the definition of the maximum pre-compression.

Fig. 4a, 4b, and 4c show the results of the FEM analysis, in terms of stress, for the samples previously described. To evaluate the stress, a force acting vertically on the structure positioned in correspondence with the path created for the insertion of the cable was simulated. This force, which simulates the TSA, has sufficient intensity to realize displacements comparable to those observed experimentally. It is indicated by the blue arrow in Fig. 4d. Furthermore, to simulate the tendon used to bend the finger, a force, indicated

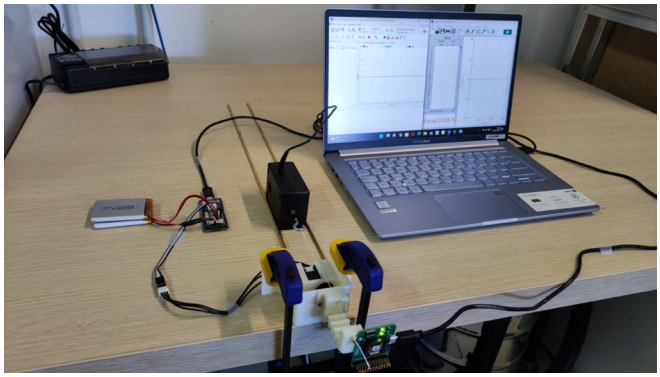

Fig. 5: Experimental setup for the wave-joint stiffness characterization.

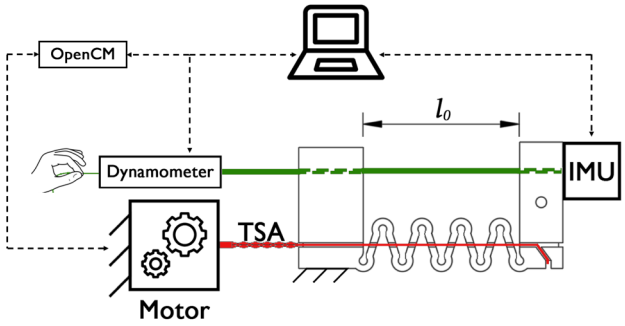


Fig. 6: Experimental setup for joint characterization scheme. In the test, the actuation force, exerted by an experimenter, is measured by a dynamometer, while the joint bending angle is measured by an IMU. For each test, the length of the joint is controlled by the TSA.

with the red arrow in Fig. 4c, with an intensity equal to $5\,\mathrm{N}$ was vertically applied to the cube edge in correspondence to the other tendon path. The constrained part is still the same: the base cube of the wave-shape joint.

It is worth noticing that the maximum equivalent stress that can be sustained by standard ABS is $60\,\mathrm{MPa}$. Results show that in all case study, the compliant structure is strong enough to resist in all the simulated load cases.

### C. Joint characterization: experimental setup

Concerning the joint characterization, experiments were aimed at evaluating the difference wave-joint stiffness values realized by controlling the twisted string actuator. In Fig. 5 the experimental setup is shown, while its scheme is reported in Fig. 6. The testing setup is composed of an inertial measurement unit Xsens Mi-3 (Xsens, NL) embedding an accelerometer, a gyroscope, and a magnetometer in a single chip that is mounted on the top of the finger, used to measure its orientation variation when the actuation tendon is pulled, a digital dual-range Vernier dynamometer (Vernier Software & Technology, US) with an accuracy of 0.05N and a microcontroller (OpenCM9.04, Robotis) to control the twisted tendons, actuated by a Dynamixel XL330-M077-T motor, characterized by stall torque of 0.228 Nm at $6.0\,\mathrm{V}$.

The support of the twisted string actuator was fixed to the table while a special path made with a brass bar was used to force the tester during the experiment to apply a horizontal force on the compliant module in the direction of the tendon.

The choice of placing the sample in a horizontal position instead of a vertical one allows us to compensate the gravity force that could affect the digital dynamometer during tests.

We first measured the initial length of the compliant module and, before each test, the dynamometer was positioned to have the tendon under tension.

All the samples described above have been evaluated in the same way and under the same conditions for 10 defined TSA motor currents ($\tau$) during the twisting.

Once the TSA motor reached the required $\tau$ value, the tester started to pull the tendon connected to the dynamometer, with a force in the range 1-$5\,\mathrm{N}$ with steps of $1\,\mathrm{N}$ for each torque creating a step force function profile with a time step of 5 seconds. This was repeated 3 times. Finally, for each sample, when the motor reached the maximum torque $\tau$, we measured the corresponding joint final length.

## III. Results

### A. Results of joint characterization

Data from force and IMU sensors were collected at a frequency of $100\,\mathrm{Hz}$ and then processed using MATLAB. For each step of the acquired force profile, i.e. from 1 N to 5 N, the average was evaluated and associated with the corresponding average step profile containing the angles. In Fig. 7 the results for the five most representative $\tau$ values, for the three joint samples, have been reported. The three diagrams correspond to the three representative joints previously introduced, with $n_r = 3, 4, 5$, respectively. In each diagram, the rotation angle measured by the IMU sensor is reported as a function of the force applied to the tendon, measured by the dynamometer, each curve is obtained by actuating the TSA with a certain $\tau$. It is worth noticing that, as expected, as the $\tau$ increases, the bending angle decreases, indicating that the joint stiffness increases. It's also interesting to notice that the force/angle behavior is approximately constant for the first four $\tau$ values. This aspect is interesting since it means that, for lower values of joint pre-compression, joint stiffness is approximately constant over a wide range of rotation angles. As the pre-compression increases, the force/angle curve presents evident non-linear (stiffening) behavior, that can be motivated by the relevant crushing of joint waves. Finally, by comparing the results obtained with the three samples, it is evident how joint stiffness decreases as the length of the joint increases.

### B. Feasibility example with a three-phalanges finger

In addition to the three different samples of compliant joints with variable stiffness, we also designed an additive

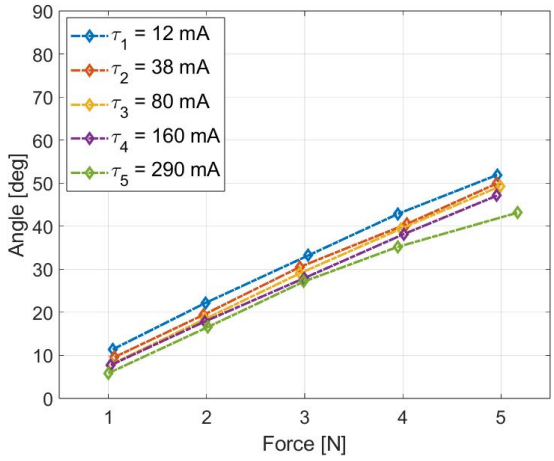


(a)

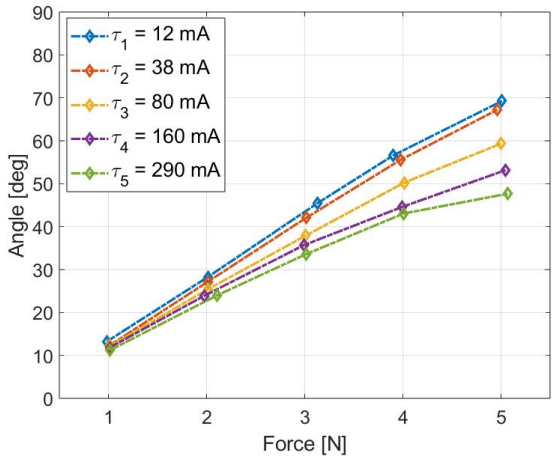


(b)

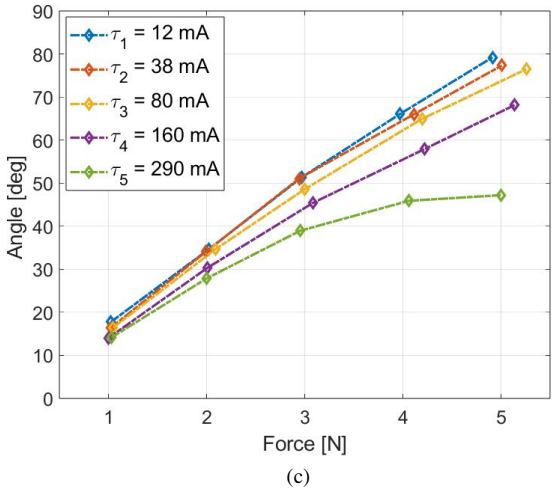


(c)

Fig. 7: Results of the joint characterization for different values of $\tau$. (a) $n_r = 3$; $l_0 = 30\,\mathrm{mm}$; $l_f = 24\,\mathrm{mm}$. (b) $n_r = 4$; $l_0 = 36\,\mathrm{mm}$; $l_f = 28\,\mathrm{mm}$. (c) $n_r = 5$; $l_0 = 42\,\mathrm{mm}$; $l_f = 30\,\mathrm{mm}$.

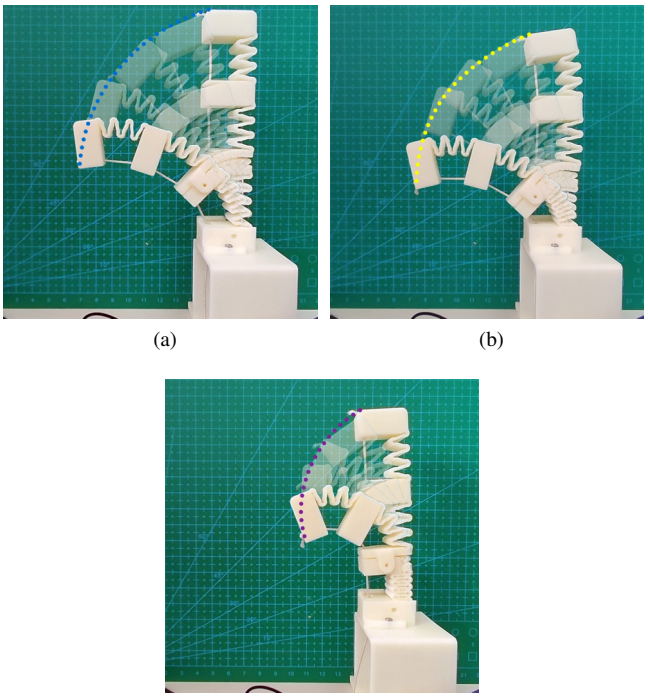

(a) (b)

(c)

Fig. 8: Trajectories followed by the fingertip in the three cases: (a) normal stiffness ($\tau = 0\,\mathrm{mA}$); (b) medium stiffness($\tau = 150\,\mathrm{mA}$); (c) maximum stiffness ($\tau = 390\,\mathrm{mA}$).

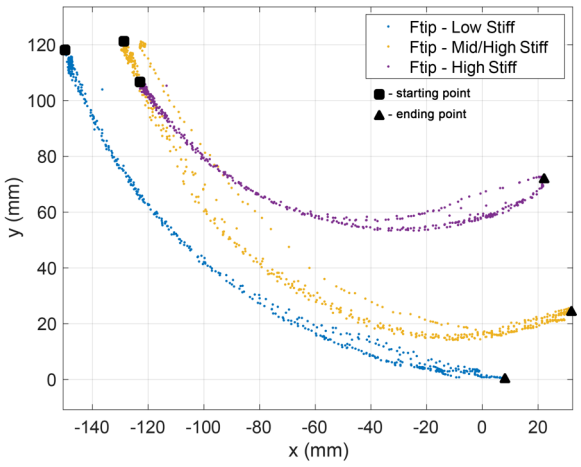


Fig. 9: Superposition of the cloud points obtained tracking the fingertip in the tests shown in Fig. 8, during the finger flexion movement.

module that can be assembled on them, to obtain a structure with three phalanges and three joints that could constitute the finger element of a gripper or a compliant robotic hand. As detailed in [9], passive joint stiffness has a fundamental role in tendon driven underactuated robotic fingers in defining closure trajectory. In that work, this feature has been exploited in the design phase, and a procedure for synthesizing joint mechanical features on the basis of gripper requirements has been presented. In the finger presented in this work, the stiffness can be further regulated by acting on the TSA, as previously detailed. In the second set of experiments we therefore analyzed how fingertip trajectory, and consequently finger closure movement, can be varied by acting on the stiffness of the proximal joint.

As can be seen in Fig. 2b, there is a hole on the top part of the rigid element, which is introduced to host the interchangeable module. The module that we designed for this purpose, is made up of two phalanges, with $n_r = 3$.

The final prototype, with which we evaluated the trajectories, is shown in Fig. 8. For the controlled-stiffness joint. We analyzed the closure motion of the finger obtained in three cases: normal stiffness (no TSA action), medium stiffness and maximum stiffness. To track the fingertip trajectories, we used Tracker, an open-source software for video analysis and modeling. Specifically, the motion of the upper front edge of the rigid distal element was tracked. Fig. 8a, Fig. 8b, and Fig. 8c, show the superposition of five frames of the normal, medium, and maximum stiffness, respectively, during the finger flexion motion, while Fig. 9 reports on the finger reference flexion plane, the fingertip trajectories achieved by changing the stiffness of the first compliant module.

## IV. Discussion

In this paper, we presented a possible solution for controlling flexural joint stiffness in underactuated tendon-driven robotic finger, based on the application of a controllable joint pre-compression by means of a TSA. We introduced the features of the joint and then performed an identification of its force/deflection behavior in different operative conditions. Finally, we showed how by regulating the stiffness in the proximal joint of a finger composed of three modules we can obtain different fingertip trajectories.

The proposed solution presents some improvements with respect to previous works on this topic, as for instance those proposed in [9]–[11]. The proposed finger structure still has a modular and monolithic structure, but it is possible to actively change joint stiffness and therefore the overall closure motion and grasping properties. Stiffness regulation is obtained by adding an active system to the joint that applies a controlled pre-compression to gripper elastic joints.

The pre-compression is realized with a TSA-based actuator, that is particularly compact. Stiffness regulation does not require high dynamics properties, so the TSA motor can be sufficiently small to be easily embedded inside the rigid parts of the modules composing the finger.

The finger maintains a modular structure, in which, depending on the specific application, it is possible to preliminarily define which joints should have a variable stiffness and the ones in which it can be maintained constant, so as to keep as limited as possible the number of actuators. Previous works, as for instance in [9], showed in particular that in a soft-rigid structure, the joint whose stiffness mostly influences the closure motion is the proximal one. Activating the stiffness of the proximal joint does not significantly increase finger mechanical complexity, since the TSA motor is on the base structure of the finger.

One of the main observation that could arise from the proposed work is that adding a TSA actuator for regulating the stiffness in an underactuated gripper goes in a direction apparently opposite with respect to the simplification and adaptability provided by soft robotics. Concerning this aspect, we already observed the possibility of regulating passive joint compliance could be provided to a limited number of joints only, preferably the proximal ones. The increase of complexity, in this case, is not so critical. Furthermore, in some cases in which the presence of actuators and electronics components close to the fingers could be a problem (e.g. in food handling, underwater manipulation, etc.), and if such a regulation is required *una tantum*, stiffness regulation could be realized manually, for instance by means of a screw.

It's worth observing also that adding a pre-compression to the joint increases the overall stress status of the joint and could lead to mechanical failures or mechanical fatigue. This issue should be further investigated in future developments of this work and could be mitigated by using fatigue-resistant materials.

Besides the stiffness, adding a pre-compression to the wave-joint also produces a change in joint length and an overall variation of finger dimensions. This effect could be properly managed by a robot arm control system or by the grasp planner. Moreover, rather than a drawback, this effect could be an opportunity and further exploited in in-hand manipulation tasks, for instance developing algorithms inspired by the caterpillar locomotion strategy [16], [17].

Finally, in the preliminary tests that we presented in this paper, we controlled independently finger actuation and stiffness regulation of a single finger. In future developments of this work, we will introduce this type of joint in a multi-fingered gripper, and we will further investigate how tendon actuation and joint stiffness regulation can be dynamically combined.

## References


[1] J. Shintake, V. Cacucciolo, D. Floreano, and H. Shea, "Soft robotic grippers," *Advanced materials*, vol. 30, no. 29, p. 1707035, 2018.

[2] C. Della Santina, M. G. Catalano, A. Bicchi, M. Ang, O. Khatib, and B. Siciliano, "Soft robots," *Encyclopedia of Robotics*, vol. 489, 2020.

[3] R. Deimel and O. Brock, "A novel type of compliant and underactuated robotic hand for dexterous grasping," *The International Journal of Robotics Research*, vol. 35, no. 1-3, pp. 161–185, 2016.

[4] A. K. Nguyen, A. Russell, N. Naclerio, V. Vuong, H. Huang, K. Chui, and E. W. Hawkes, "A tri-stable soft robotic finger capable of pinch and wrap grasps," in *2020 IEEE International Conference on Robotics and Automation (ICRA)*. IEEE, 2020, pp. 9028–9034.

[5] R. Deimel and O. Brock, "Soft hands for reliable grasping strategies," in *Soft Robotics*. Springer, 2015, pp. 211–221.

[6] M. Pozzi, S. Marullo, G. Salvietti, J. Bimbo, M. Malvezzi, and D. Prattichizzo, "Hand closure model for planning top grasps with soft robotic hands," *The International Journal of Robotics Research*, vol. 39, no. 14, pp. 1706–1723, 2020.

[7] V. Ruiz Garate, M. Pozzi, D. Prattichizzo, and A. Ajoudani, "A bio-inspired grasp stiffness control for robotic hands," *Frontiers in Robotics and AI*, vol. 5, p. 89, 2018.
[8] M. R. Cutkosky *et al.*, "On grasp choice, grasp models, and the design of hands for manufacturing tasks." *IEEE Transactions on robotics and automation*, vol. 5, no. 3, pp. 269–279, 1989.
[9] G. Salvietti, I. Hussain, M. Malvezzi, and D. Prattichizzo, "Design of the passive joints of underactuated modular soft hands for fingertip trajectory tracking," *IEEE Robotics and Automation Letters*, vol. 2, no. 4, pp. 2008–2015, 2017.
[10] I. Hussain, O. Al-Ketan, F. Renda, M. Malvezzi, D. Prattichizzo, L. Seneviratne, R. K. Abu Al-Rub, and D. Gan, "Design and prototyping soft–rigid tendon-driven modular grippers using interpenetrating phase composites materials," *The International Journal of Robotics Research*, vol. 39, no. 14, pp. 1635–1646, 2020.
[11] M. Dragusanu, G. M. Achilli, M. C. Valigi, D. Prattichizzo, M. Malvezzi, and G. Salvietti, "The wavejoints: a novel methodology to design soft-rigid grippers made by monolithic 3d printed fingers with adjustable joint stiffness," in *2022 International Conference on Robotics and Automation (ICRA)*. IEEE, 2022, pp. 6173–6179.
[12] G. Palli, C. Natale, C. May, C. Melchiorri, and T. Wurtz, "Modeling and control of the twisted string actuation system," *IEEE/ASME Transactions on Mechatronics*, vol. 18, no. 2, pp. 664–673, 2012.
[13] T. Würtz, C. May, B. Holz, C. Natale, G. Palli, and C. Melchiorri, "The twisted string actuation system: Modeling and control," in *2010 IEEE/ASME International Conference on Advanced Intelligent Mechatronics*. IEEE, 2010, pp. 1215–1220.
[14] T. Tsabedze, E. Hartman, E. Abrego, C. Brennan, and J. Zhang, "Tsabrag: A twisted string actuator-powered biomimetic robotic assistive glove," in *2020 International Symposium on Medical Robotics (ISMR)*. IEEE, 2020, pp. 159–165.
[15] D. Lee, D. H. Kim, C. H. Che, J. B. In, and D. Shin, "Highly durable bidirectional joint with twisted string actuators and variable radius pulley," *IEEE/ASME Transactions on Mechatronics*, vol. 25, no. 1, pp. 360–370, 2019.
[16] M. Rogóż, H. Zeng, C. Xuan, D. S. Wiersma, and P. Wasylczyk, "Light-driven soft robot mimics caterpillar locomotion in natural scale," *Advanced Optical Materials*, vol. 4, no. 11, pp. 1689–1694, 2016.
[17] S. Kim, C. Laschi, and B. Trimmer, "Soft robotics: a bioinspired evolution in robotics," *Trends in biotechnology*, vol. 31, no. 5, pp. 287–294, 2013.